CHALMERS
UNIVERSITY OF TECHNOLOGY

Collisional damping of spherical ice particles

Powder Technology 383 (2021) 318–327

Contents lists available at ScienceDirect

Powder Technology

journal homepage: www.elsevier.com/locate/powtec

Collisional damping of spherical ice particles

Tobias Eidevåg [a,b,*], Erik S. Thomson [c], Sofia Sollén [d], Johan Casselgren [d], Anders Rasmuson [a]

[a] Department of Chemistry and Chemical Engineering, Chalmers University of Technology, SE-41296 Gothenburg, Sweden
[b] Contamination and Core CFD, Volvo Car Corporation, SE-40531 Gothenburg, Sweden
[c] Department of Chemistry & Molecular Biology, Atmospheric Science, University of Gothenburg, SE-41296 Gothenburg, Sweden
[d] Division of Fluid and Experimental Mechanics, Luleå University of Technology, SE-97187 Luleå, Sweden

ARTICLE INFO

Article history:
Received 5 November 2020
Received in revised form 10 December 2020
Accepted 16 January 2021
Available online 22 January 2021

Keywords:
Ice adhesion
Particle impact
coefficient of restitution
Icing premelting
Surface melting

ABSTRACT

This paper presents experimental values for the coefficient of restitution (e_n) for millimeter-sized ice particles colliding with massive walls at different temperatures. Three different wall materials are tested: hardened glass, ice and Acrylonitrile butadiene styrene (ABS) polymer. The results show a high sensitivity to impact velocity V_i, where e_n decreases rapidly with increasing V_i. The results also show a decrease in e_n with increasing temperature T. A novel model that predicts e_n based on the assumption of collisional melting and viscous damping caused by an increased premelted liquid-layer, is proposed. The model predicts both the velocity and the temperature trends seen in the experiments. The difference obtained in experiments between wall materials is also captured by the new model. A generalized regime map for ice particle collisions is proposed to combine the new model with previous work.

1. Introduction

Collisions of ice particles are important in many physical systems. A deep understanding of these collisions is important to model and predict how systems of ice particles will develop in time. Examples of such systems are ice particles in space that agglomerate, which is an important part of planet formation [1]; and ice particles in the atmosphere that transfer charge through collisions, thereby triggering thunderstorms [2] or grow and precipitate from the sky as snow and/or rain [3]. Snow and ice tend to accumulate on surfaces, such as buildings [4], infrastructure [5], and vehicles [6]. Significant research focuses on preventing snow sticking and accumulating. A fundamental understanding of the energy dissipation in collisions between ice particles and massive walls, is thus an important part of understanding how snow or ice accumulates on surfaces.

The energy dissipation for a particle colliding with a wall is an important subject in the field of particle technology [7–10]. A well-established measure to characterize the energy dissipation for particle collisions is the coefficient of restitution e_n, which is the ratio between normal rebound velocity V_r and normal impact velocity V_i,

$$e_n = \frac{V_r}{V_i}, \tag{2}$$

where by definition it is expected that $e_n \in [0,1]$. A variety of different damping mechanisms affect the dependencies and trends of e_n, and consequently, there are many different models for e_n [11]. Examples of mechanisms that have commonly been studied are viscoelastic damping [12,13], adhesion (typically due to van der Waals forces) [14,15], plastic dissipation [16], and liquid layer damping [17–21]. The e_n has also been extensively studied for ice particles and a wide range of studies examine ice particle impacts [22–25], and Güttler et al. [26] have compiled an excellent literature survey. They summarize experimental data of particles in general and for ice particles in particular. One of the most extensive works that examines the e_n specifically for ice particles is by Higa et al. [27]. Those authors studied spherical ice particles with diameters from 2.8 to 72 mm for a variety of temperatures and impact velocities. A key finding from that study is that below a certain critical velocity, e_n is constant and independent of V_i, while above this velocity, e_n rapidly decreases with increasing V_i.

Although many studies have examined ice particle collisions, to the best of our knowledge, no data has been published on the e_n for ice particles smaller than 2.8 mm. Snow grains on the ground typically, transform from snowflakes into spherical-shaped particles through metamorphism [28], and this grains range from hundreds of microns to a few millimeters in diameter [29].

* Corresponding author at: Department of Chemistry and Chemical Engineering, Chalmers University of Technology, SE-41296 Gothenburg, Sweden.
E-mail address: tobias.eidevag@chalmers.se (T. Eidevåg).

https://doi.org/10.1016/j.powtec.2021.01.025

In this paper, we present experimental results that extend the knowledge of ice particle collisions by examining collisions of millimeter-sized ice particles with an ice wall, a hardened glass wall and an ABS polymer wall. These walls are interesting because they represent large variations in Young's modulus, and they are common surfaces on vehicles in the automotive industry. Icing of external automobile surfaces is becoming a key obstacle for automated cold-weather driving. We relate observations to previous experimental work by Higa et al. [27], and utilize a collisional melting model based on a framework proposed by Wettlaufer [30] to model collisional melting for collisions between ice particles. We arrive at a novel model for e_n that predicts a viscous loss caused by a premelted liquid layer, and we show that the model captures experimental observations. Finally, we present a regime map of the e_n for ice particles where we combine our previous work on damping due to van der Waals forces [31] with the expanded collisional model.

2. Measurements

Experiments were performed to measure the e_n for ice particles colliding with massive walls of different materials. To validate the setup, collisions of glass particles against a glass wall were also measured at the same temperatures used in the ice particle experiments and at room temperature.

2.1. Experimental setup

Ice particles were created using a previously established method whereby a mixture of distilled water and food colorant is dropped into liquid nitrogen using a syringe [32]. The syringe allowed the size of the droplets to be uniform, and the smallest available syringe needle was used to create the smallest ice particles possible. Previous studies of millimeter-sized spherical glass particles colliding with glass walls [19,33], led us to use spherical glass particles to validate the experimental setup. Glass particles with 0.5 mm, 1 mm, and 2 mm in diameter were used. Particles were picked up using a paintbrush and released into a vertical metal pipe. The particles were then accelerated to a certain impact speed V_i by gravity and collided with the massive wall placed under the pipe. The impact speed was varied by changing the length of the pipe. Ice, hardened glass, and ABS polymer were used as the massive wall materials where the ice wall was created by freezing distilled water in a silicone mold. A high-speed camera recorded each particle before and after impact and a laser connected to the camera triggered image acquisition when a particle crossed the laser beam prior to impact (Fig. 1). The experiments were recorded at 4000 frames per second. In order to focus this work on normal collisions between particles and walls, massive walls with low surface roughness were chosen to avoid tangential velocity components after impact and experimental samples with a clear tangential velocity component were removed from the data set. The experiments were conducted in a large cooling chamber with temperature control. A temperature probe used to monitor the temperature was located 20 cm from the massive wall and was used to monitor the temperature T with the mean and 1σ standard deviation to indicate uncertainty (Table 1). Recordings from the high-speed camera were analyzed to extract particle trajectories, velocities, and particle size. The image analysis was done using Fiji and the single-particle tracking tool TrackMate [34]. Before using TrackMate, images were pre-processed to improve particle detection by removing the background and masking the images. For each recorded frame, the particle diameter was calculated from the sum of the pixel area. The median of all calculated diameters were then taken to estimate the particle sizes, where median were used to eliminate outliers caused by edge effects. The trajectories resulting from the image analysis were post-processed to determine the velocity before and after each collision. The uncertainty in position was quantified by manually measuring the center positions

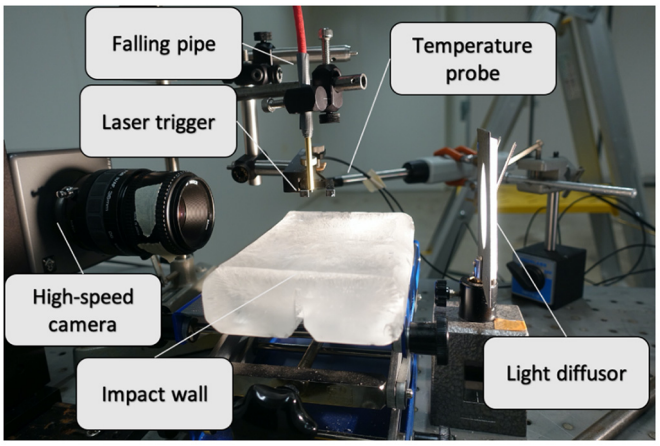

Fig. 1. Experimental setup.

$$\delta e_n = \sqrt{\left(\frac{\delta V_i}{V_i}\right)^2 + \left(\frac{\delta V_r}{V_r}\right)^2}\, e_n. \tag{2}$$

of particles and averaging the deviation between these measurements and the output of the tracking tool. The obtained average positional uncertainty $\delta x = 2.613 \cdot 10^{-5}$ m results in an velocity uncertainty $\delta V = 0.105$ m/s. The uncertainty in the coefficient of restitution, δe_n, is then calculated by further propagation of uncertainties as

Fig. 2 illustrates an ice particle colliding with a glass wall with the particle's center point trajectory extracted from the image analysis overlayed as circles.

For particle impacts that occur close to the bulk material melting temperature there is the potential that proximity to the melting temperature T_m plays an important role in the collisions. Thus the homologous temperature $T_H = T/T_m$, where T is the experimental temperature, is often used to depict how close to the melting point the experiments come.

2.2. Experimental observations

The e_n obtained for glass particles colliding with glass walls is shown in Fig. 3 as a function of V_i. A melting temperature of $T_m = 1300$K is used for glass particles to calculate T_H and these measurements detected no difference for the e_n at different temperatures, or for varying V_i. The mean e_n was found to be 0.94 ± 0.05 at the 2σ level.

An empirical function for e_n proposed by Higa et al. [27] for ice particles impacting an ice wall is,

$$e_n = \begin{cases} e_{qe}\left(\dfrac{V_i}{V_c}\right)^{-\ln(V_i/V_c)} & V_i \geq V_c, \\ e_{qe} & V_i < V_c, \end{cases} \tag{3}$$

Table 1
Experimental parameters, wall material, T and T_H; and the resulting e_{qe} and V_c extracted from fitting experimental data.

Impact wall	T [K]	T_H [−]	e_{qe}	V_c [m/s]
glass	254 ± 1	0.930	0.74 ± 0.02	1.60 ± 0.07
	262 ± 1	0.959	0.67 ± 0.03	1.38 ± 0.07
ice	254 ± 1	0.930	0.82 ± 0.02	1.90 ± 0.10
	262 ± 1	0.959	0.79 ± 0.04	1.62 ± 0.16
	267 ± 1	0.977	0.66 ± 0.05	1.39 ± 0.13
abs polymer	254 ± 1	0.930	0.86 ± 0.05	>2.8
	262 ± 1	0.959	0.89 ± 0.02	>3.1

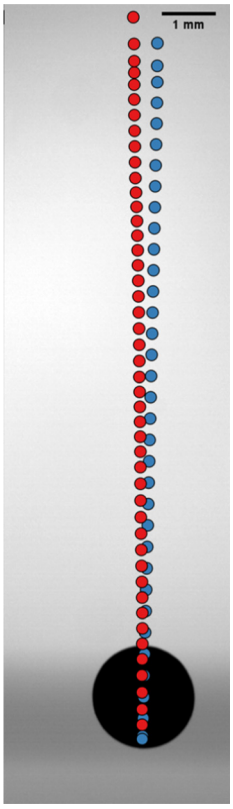

Fig. 2. Snapshot of an ice particle colliding with a glass wall with extracted trajectories from the image analysis. Blue circles show the approaching path, with red circles illustrating the path of the rebounding particle.

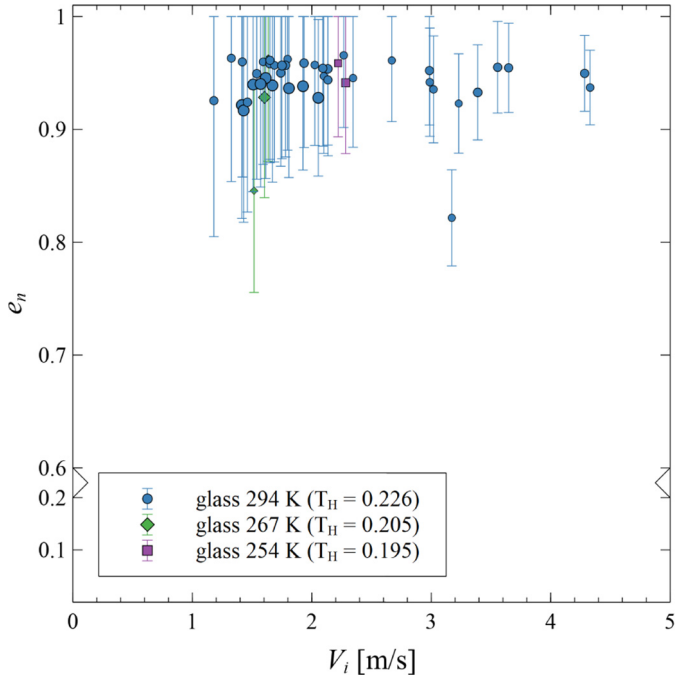

Fig. 3. The e_n of glass particles colliding with a glass wall as a function of impact velocity at three different temperatures. The error bars represent the propagated uncertainty δe_n.

where e_{qe} is the coefficient of restitution in the quasi-elastic regime, and V_c is the critical velocity and suggests e_n varies only above V_c. Measurements of ice particles colliding with an ice wall were

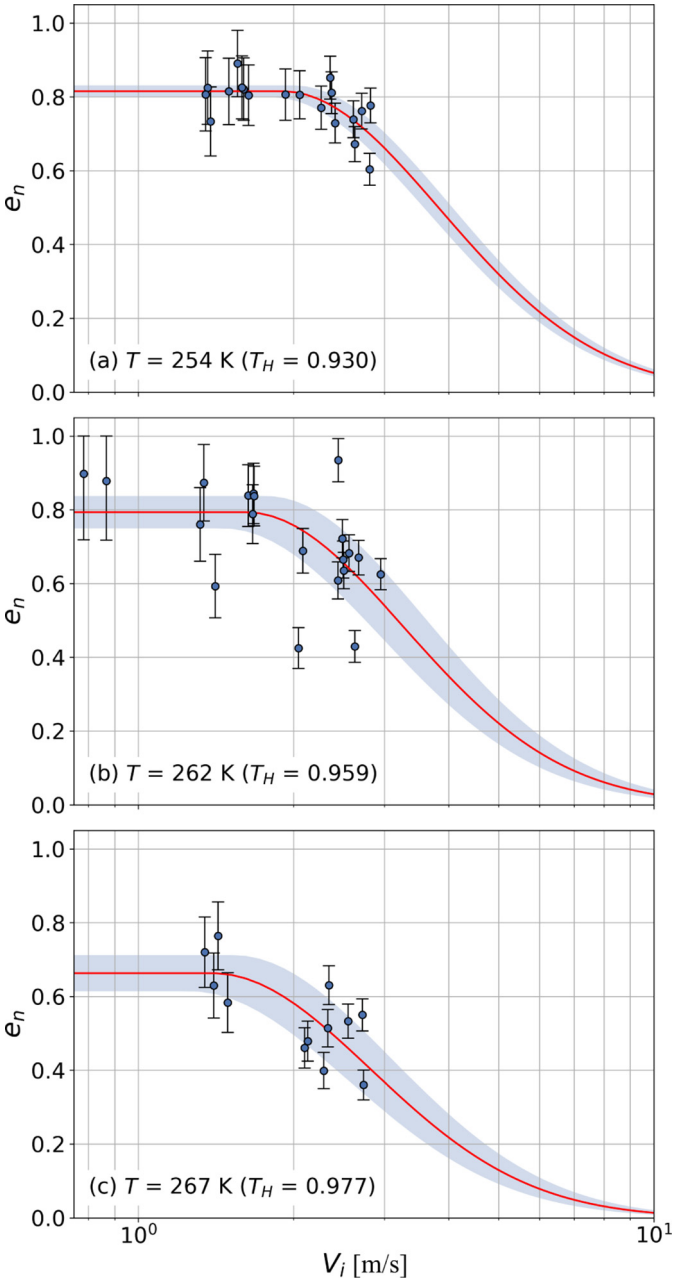

Fig. 4. The e_n for ice particles colliding with an ice wall as a function of V_i. The error bars represent δe_n. The line shows the non-linear least square fit of e_n as a function of V_i. The shaded area shows the propagated uncertainty of e_n based on the matrix square root of the covariance matrix from the non-linear fit of V_c and e_{qe}.

conducted at three temperatures: 267 K, 262 K, and 254 K, which correspond to T_H of 0.977, 0.959 and 0.930 respectively. The ice particles had an average diameter of 1.64 ± 0.15 mm. Fig. 4 shows the measured e_n values with a non-linear least square fit of Eq. (3) superimposed. The uncertainties of the fitted V_c and e_{qe} are quantified as the matrix square roots of the covariance matrix from the non-linear fit.

Collisions of ice particles with a glass wall were measured at two temperatures: 254 K and 262 K. The resulting measurements of e_n are shown in Fig. 5.

Similar to the experiments with a glass wall, measurements of ice particles colliding with an ABS polymer wall were conducted at two temperatures: 254 K and 262 K. The extracted e_n are shown in Fig. 6, where it appears that for all observations that $V_i < V_c$.

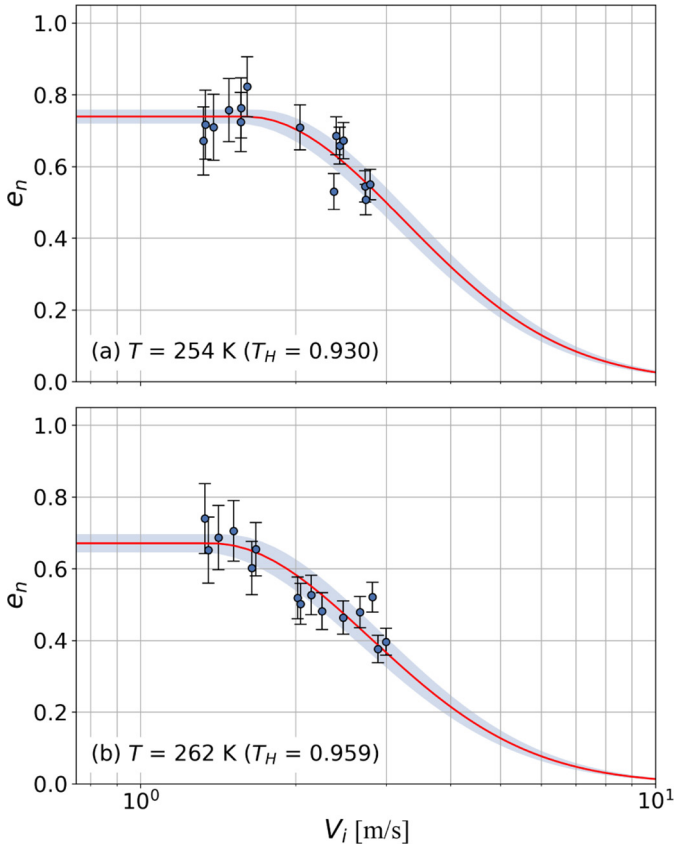

Fig. 5. The e_n for ice particles colliding with a glass wall as a function of V_i. The error bars represent δe_n. The line shows the non-linear least square fit of e_n as a function of V_i. The shaded area shows the propagated uncertainty of e_n based on the matrix square root of the covariance matrix from the non-linear fit of V_c and e_{qe}.

A summary of the fitted parameters e_{qe} and V_c are shown in Table 1 in addition to the uncertainties estimated from the coviarance matrix.

The confidence interval for both e_{qe} and V_c in our experimental observations for ice particles colliding with an ice wall at $T = 262$ K are either very close to or overlap with the confidence intervals for the two parameters at $T = 254$ K and $T = 267$ K. A comparison of results for the experiments involving massive walls of ice and glass shows that the e_n is lower for the glass wall than the ice wall. This is also reflected in the obtained parameters V_c and e_{qe}. For all experiments except those with the ABS polymer, a clear trend was obtained where e_n decreased with increasing T_H. This is maybe not surprising given the fact that T_H is greater than 0.9, which are temperatures that are very close to the melting point of water.

2.3. Comparison with previous experimental results

The values of e_n obtained for glass particles colliding with a glass wall shown in Fig. 3 are similar to previous findings [19,33] that found e_n to range from 0.92 to 0.98. Since the experimental conditions were far from the melting temperature of the glass particles, with $T_H \approx 0.2$, we did not expect to see a difference between temperatures, and the values obtained imply that the experimental equipment was not affected operating in cold temperatures. Ice particles colliding with both glass and ice surfaces behave differently, which is also expected given that $T_H > 0.9$ in our observations.

Fig. 4 shows that Eq. (3) captures the rapid trend of a decrease in e_n with increasing V_i above the critical velocity V_c. An empirical equation for the critical velocity V_c was derived in Higa et al. [27] as a function of temperature and particle radius R. If we simplify this equation it can be re-expressed as,

$$V_c = K_1 \exp\left(\frac{K_2}{k_b T}\right) R^{-0.5}, \tag{4}$$

where k_b is the Boltzmann constant, and K_1 and K_2 are constants extracted from the Higa et al. [27] results ($K_1 = 7.0055 \cdot 10^{-7}$ and $K_2 = 0.25$).

Fig. 7 shows the V_c predicted by Eq. (4) for the three temperatures used in the ice particle collision experiments with an ice wall. The figure also shows the values obtained for V_c from Table 1 and the values from Higa et al. [27] obtained at $T = 261$ K.

3. Collisional damping of ice particles

3.1. Collisional melting - Premelting due to an impact

The present work and the previous Higa et al. [27] experiments show that the e_n, for ice particles colliding with massive walls, significantly decreases with increasing V_i above certain velocities. For obtained values of $V_c \approx 1$ m/s, the velocity dependency of e_n is close to V_i^{-1}, which is significantly more rapid than plastic dissipation models predict for e_n, which are typically proportional to $V_i^{-1/4}$ [35]. Interestingly, this strong dependency has been seen before. A study of micrometer-sized metal particles colliding with a metal surface [36] found that the metal particles follow the plastic dissipation dependency of $V_i^{-1/4}$ for low velocities ($V_i \leq 10$ m/s). At high velocities (100–1000 m/s), however, e_n begins to follow V_i^{-1}, the same dependency found in this work for ice particles. However, those experiments were performed at room temperature meaning at low T_H for the metal. Given that the T_H in these ice particle experiments is close to unity it is not surprising that e_n for ice particles begins to fall at lower velocities since the material will be more sensitive to melting. Sensitivity to T_H has been observed for other materials, for example, in a recent study where steel balls collide with heated metal walls, Hashemnia [37] shows that e_n begins to decrease rapidly for $T_H > 0.6$. Another study of glass particles colliding with a PEG (Poly Ethylene Glycol) substrate reported that e_n fell to zero as the substrate approached its melting temperature [38].

As shown in Fig. 7 the empirical equation for V_c (Eq. (4)) predicts that V_c decreases with increasing T_H. However, physical reasoning suggest that V_c should approach 0 m/s as $T_H \to 1$, which implies that something fundamental is missing in Eq. (4). We propose that the damping observed for ice particles can be explained by collisional melting and specifically an increase in premelting of a liquid layer on the ice surface due to the collision. The existence of equilibrium liquid-like layers on ice surfaces is well documented [39–44], and here we expect the collision to enhance the existence of that layer. Such films are often referred to as premelted layers, quasi-liquid layers (QLL) or distorted liquid-like materials, and the material properties of the liquid layers are not necessarily expected to be those of the bulk liquid.

Models have been proposed for ice particle collisions that predict an increased premelting due to a collision [2]. Wettlaufer [30] proposed a theoretical model for collisional fusion as an explanation for the rapid damping of ice particles observed by Higa et al. [27]. That model assumes that a fraction ξ of the kinetic energy will damage the interface, and the resulting disorder causes an enhanced premelted liquid layer. This liquid layer can subsequently freeze during impact, causing the particle to fuse with the colliding object at certain velocities. The model is intended to predict fusion between ice grains at astrophysically relevant temperatures and pressures.

While fusion is relevant for astrophysical conditions with short freezing times, for our operating conditions with temperatures

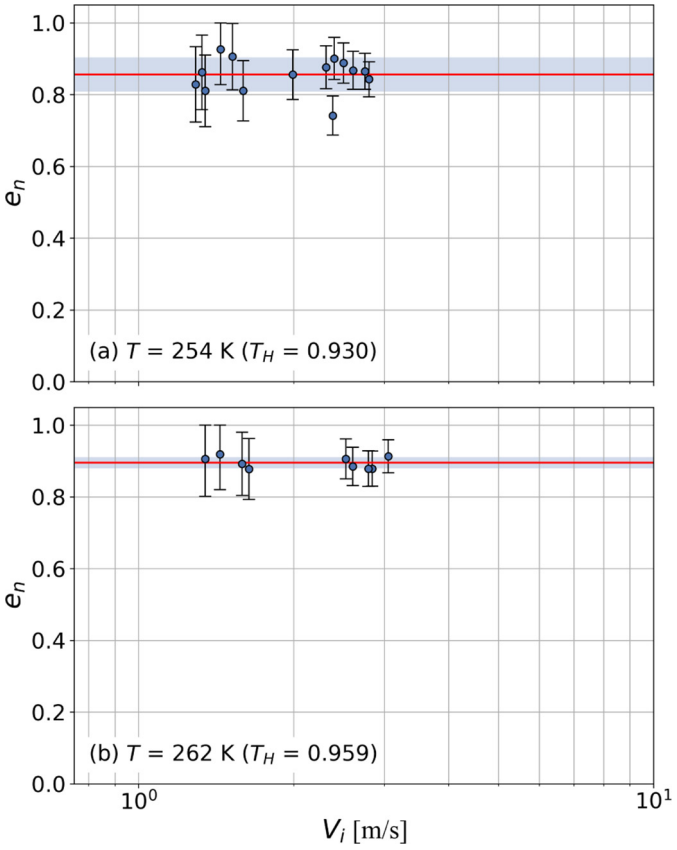

Fig. 6. The e_n for ice particles colliding with an ABS polymer wall as a function of V_i. The error bars represent δe_n. The line shows the non-linear least square fit of e_n as a function of V_i. The shaded area shows the propagated uncertainty of e_n based on the matrix square root of the covariance matrix from the non-linear fit of V_c and e_{qe}.

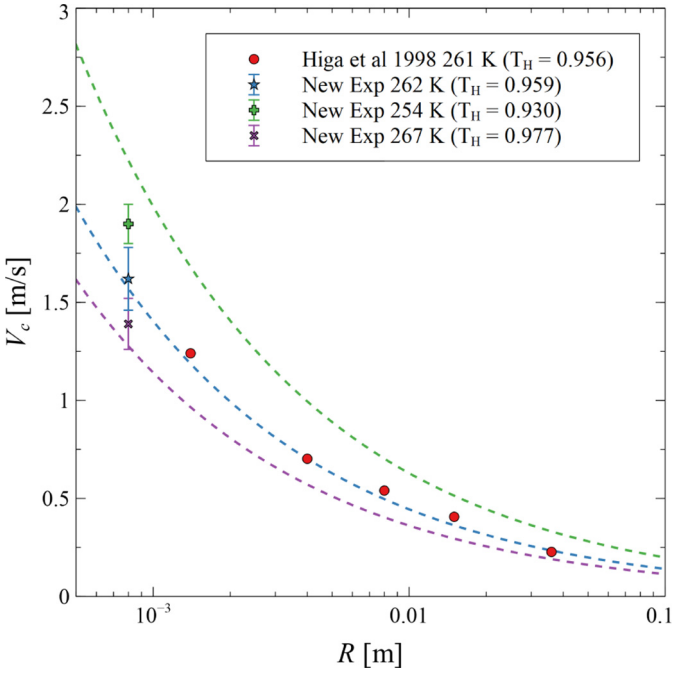

Fig. 7. Critical velocity V_c for ice particles colliding with a massive ice wall, results in this work together with previous experiments by Higa et al. [27], and the predicted V_c as a function of size for 262, 254, and 267 K. Dashed lines from Eq. (4) where the constants K_1 and K_2 are extracted from Higa et al. [27].

significantly closer to the melting point of water, fusion cannot explain the observed temperature trend. Specifically, with increasing T_H, the time scale for freezing by heat conduction is decreasing and at the same time the predicted d is increasing. This means that with increasing T_H the rate of freezing is reduced while the amount of liquid to freeze is increasing. The experimental measurements show that the damping consistently increases with increasing temperature for both the ice walls and the glass walls. We therefore argue that the associated energy loss instead can be explained by the presence of an increased liquid-layer and the associated energy loss this layer causes.

An equation for the liquid layer thickness d caused by ice particles colliding with other ice particles was derived by Wettlaufer [30]. By simplifying Eq. (3) in Wettlaufer [30] for ice particles colliding with walls we obtain,

$$d = \left(\frac{16\sqrt{6}E^*}{135\pi}\right)^{2/5} \frac{\xi\rho_s^{3/5}V_i^{6/5}R}{\left(\frac{q}{T_m}(T_m - T) + \frac{(\rho_l-\rho_s)}{\rho_s}\left(P_m(T) - \xi\left(\frac{40\rho_s V_i^2 E^{*4}}{\pi^4}\right)^{1/5}\right)\right)}. \quad (5)$$

Here ρ_s and ρ_f are the density of solid and liquid water. T_m and P_m are the bulk melting temperature and pressure for water. E^* is the effective Young's modulus in the collision defined as,

$$\frac{1}{E^*} = \frac{1-\nu_1^2}{E_1} + \frac{1-\nu_2^2}{E_2}, \quad (6)$$

where E_i and ν_i are the Young's modulus and Poisson's ratio for material i. The damage term ξ is used to describe how microscopic and mesoscopic changes lead to the deterioration of macroscopic material properties [45]. With this new formulation for d we make two interesting observations: 1) d is predicted to be linearly proportional to R, which means that the ratio, d/R, is independent of particle size. 2) d is proportional to $E^{*2/5}$, which means that increased melting should be observed with increasing Young's modulus of the material walls. To illustrate how the liquid layer changes with V_i, Fig. 8 shows the predicted d for ice particles upon impact with an ice wall as a function of V_i for the temperatures 267 K, 262 K, and 254 K. The critical velocities found in this work are highlighted in the figure. The figure shows a rapid increase in d for velocities above V_c and d is predicted to be a few microns. The secondary y-axis in the figure shows d/R, and we can see that the liquid layer thickness ranged from 0.2% to 0.4% of particle radius R around V_c. In these predictions $\xi = 0.15$ is used based on the work by Wettlaufer [30]. The uncertainty of ξ will be discussed later in this section. The energy loss for a particle-wall collision with the presence of a liquid layer has been the subject of many studies. In Crüger et al. [33], the authors observed that the e_n decreases for glass particles colliding with a wetted glass wall with increased liquid layer thickness. Matthewson [46] studied the adhesion of spheres due to a thin

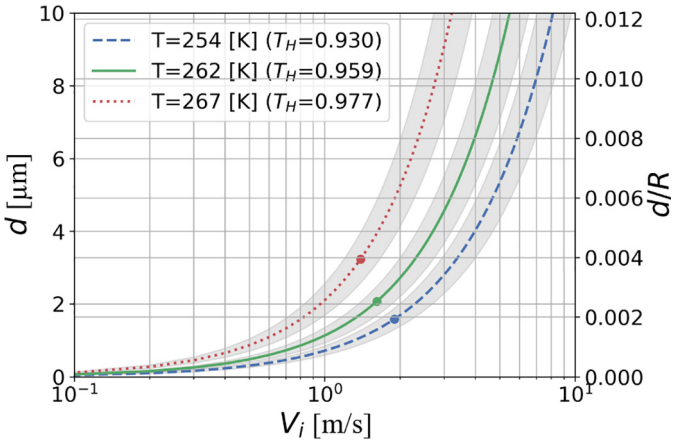

Fig. 8. Predicted d for ice particles colliding with an ice wall. The points show the critical velocities V_c obtained from the experiments in this work. The lines show d and d/R for $\xi = 0.15$, with the shaded areas showing how d and d/R vary for $\xi = 0.15 \pm 0.025$.

liquid film, and show that the adhesive force can be divided into two components: a meniscus force and a viscous damping force. While the resulting energy loss for the meniscus force is expected to be constant for a specific particle size and independent of V_i, the viscous damping loss depends on d, V_i, and the viscosity η of the fluid. We, therefore, argue that the viscous damping force will dominate for the case of damping caused by an increased premelted liquid layer. Based on Reynolds lubrication theory it has been shown by Chan and Horn [47] and Matthewson [46] that the viscous force F_v can be expressed as a function of the particles approaching velocity V and the separation distance x between the particle and the wall as,

$$F_v = 6\pi\eta R^2 h(x) V, \tag{7}$$

where $h(x)$ is a function that depends on the wetting conditions in the collision. For a particle colliding with an infinite wetted wall with constant d, Chan and Horn [47] showed that,

$$h(x) = \frac{1}{x}, \tag{8}$$

which is valid except for very thin films or when x tends to zero (when the two solid surfaces come closer to contact). The resulting energy loss E_v, for a particle colliding with an infinite wetted wall was estimated by Sutkar et al. [20] to be

$$E_v = \oint F_v dx = \frac{3}{2}\pi\eta R^2 V_i \ln\left(\frac{d}{\varepsilon}\right), \tag{9}$$

where the path integral is defined as the collision trajectory and ε is the particle roughness. In our situation the wetting area is finite and the thickness d is increasing during the course of collision (due to melting). This means that we expect $h(x)$ to be more complex than for an infinite wetted wall with constant d. It is however reasonable to expect that the resulting E_v would take a similar form as Eq. (9) and therefore we propose

$$E_v \propto \eta(T) R^2 V_i (d/\varepsilon)^a, \tag{10}$$

where the constant a can be empirically determined. The total energy loss E_t is then

$$E_t = E_v + \xi E_i, \tag{11}$$

where E_i is the initial kinetic energy and thus ξE_i is the amount of energy that causes damage to the ice particle surface. The E_t can also be expressed as a function of e_n as

$$E_t = E_i(1 - e_n^2). \tag{12}$$

We determine a using nonlinear curve fitting of the observed energy loss represented by Eq. (3). For our experimental values we find an average best fit of $a = 1.46$ for ice particles colliding with an ice wall, and therefore propose that $a = 1.5$ (or $a = 3/2$).

The premelted liquid layer is a distorted region with properties between solid and bulk liquid water [41], therefore, η is unknown but likely temperature dependent. The temperature dependent viscosity of a liquid can be expressed as,

$$\eta \propto \exp\left(\frac{G_0^+}{k_b T}\right), \tag{13}$$

where G_0^+ is a potential energy barrier empirically determined by fitting experimental data [48]. Using this we can express the viscous energy loss E_v for an ice particle colliding with a massive wall as,

$$E_v = C \exp\left(\frac{G_0^+}{k_b T}\right) V_i R^2 (d/\varepsilon)^{1.5}, \tag{14}$$

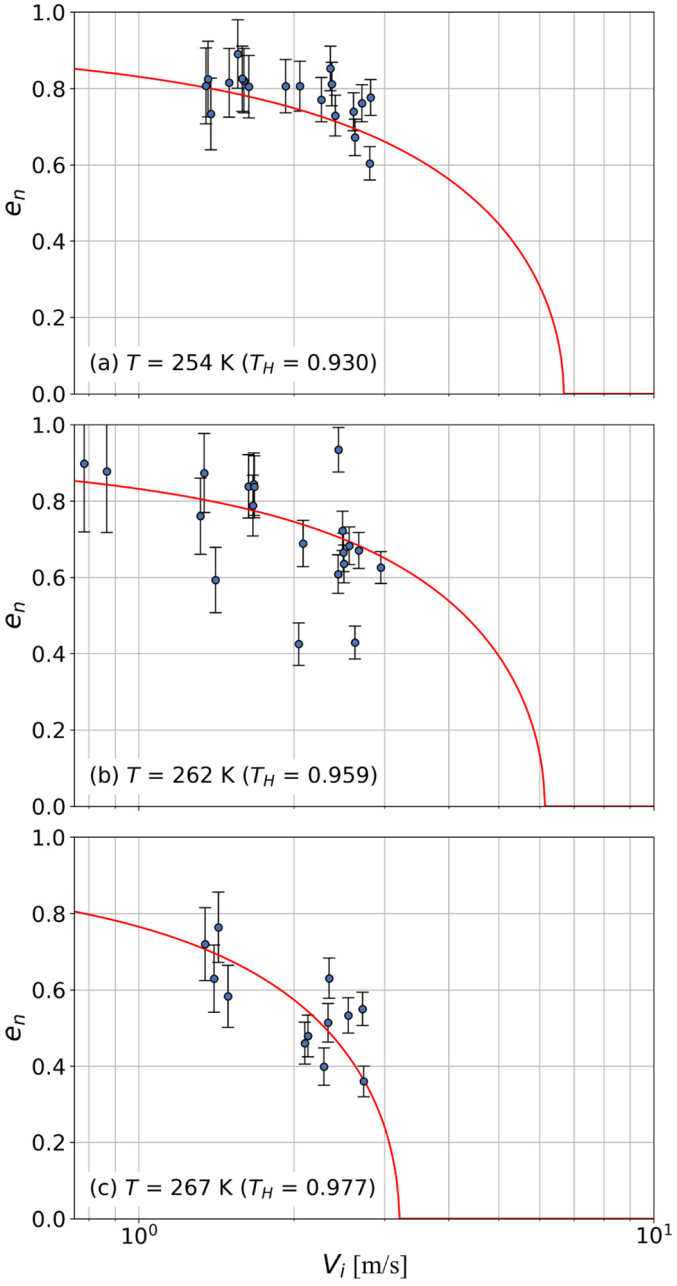

Fig. 9. Predicted e_n according to liquid layer damping together with experimental results for ice particles colliding with an ice wall as a function of V_i. The error bars represent the propagation of uncertainty for measured e_n.

where C and G_0^+ are coefficients with units Pa·s and eV, respectively. Here C represents the combined value of all constants in Eq. (10). The resulting coefficient of restitution can then be expressed as,

$$e_n = \sqrt{\frac{E_i - E_v - \xi E_i}{E_i}}. \tag{15}$$

Fitting the coefficients C and G_0^+ to the experimental data from ice particles colliding with an ice wall at $T = 267$ K and $T = 254$ K we obtained average values for $C = 0.5 \cdot 10^{-10}$ Pa·s and $G_0^+ = 0.5$ eV. The best fit gives remarkably similar results for the experiments at $T = 267$ K and $T = 254$ K with only a difference of 0.6% and 0.5% for

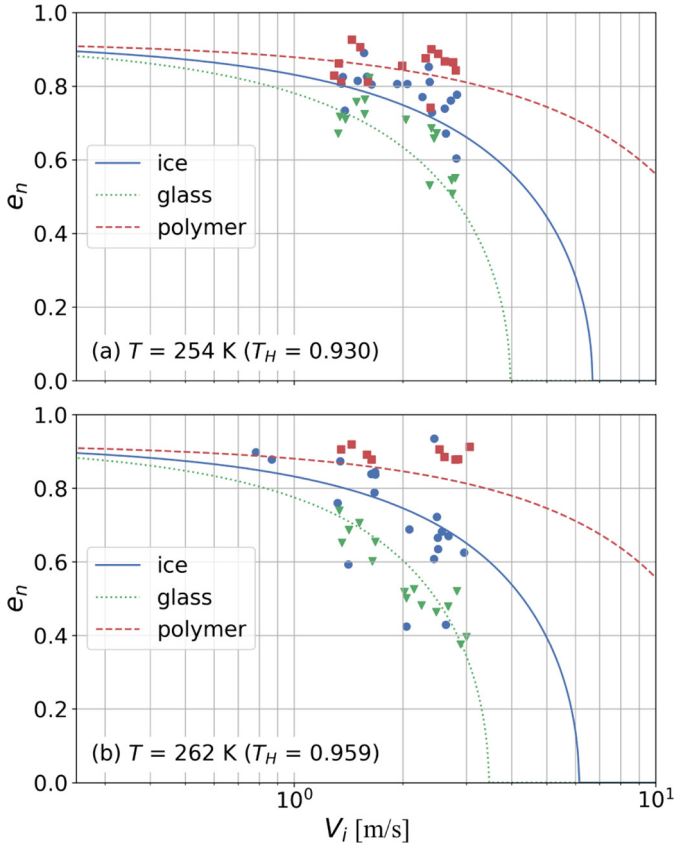

Fig. 10. The e_n for ice particles colliding with different massive walls as a function of V_i. Solid, dashed and dotted lines show predicted e_n caused by collisional melting for ice particles colliding with an ice wall, a polymer wall and a glass wall respectively. Marker symbols (Circle, square and triangle) show experimental measurements for ice particles colliding with an ice wall, a polymer wall and a glass wall respectively.

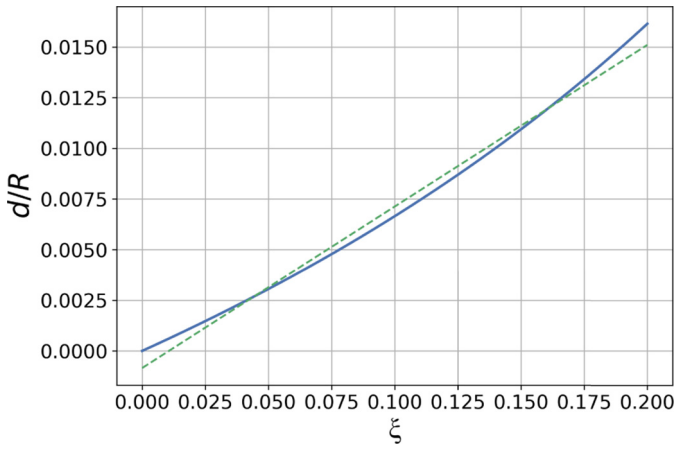

Fig. 11. Liquid layer thickness ratio d/R as a function of ξ. The blue solid line shows the predicted values of d/R for $V_i = 5$ with the straight green dashed line used to illustrate the linearity.

C and G_0^+, respectively. Fig. 9 shows the predicted coefficient of restitution for ice particles colliding with an ice wall together with the experimental measurements from the present work. As shown in the figure, the new formulation for the energy loss captures the rapid increase of energy dissipation with increasing V_i, and also captures the difference between temperatures. The new model predicts that e_n approaches zero for a finite value of V_i which is different from Eq. (3) where e_n only approaches zero as $V_i \to \infty$.

In Fig. 10 the model predictions of e_n for different wall materials and the experimental measurements for these wall materials are presented. The different wall materials are represented by different values of E^* where the material properties for the different walls are the same as used in a previous study [31] except that the Young modulus for ice is calculated as the function of temperature as in Hobbs [49]. Notably the new model predicts the trend between wall materials that is observed in the experiments.

The Eq. (15) solutions are plotted in Figs. 9-10 with $\xi = 0.15$. However, the value of ξ is not well defined and Wettlaufer [30] bounded ξ between 0.1 and 0.2. The dependency of ξ on d in Eq. (5) is almost linear for the range of velocities examined herein. Therefore, changes in ξ will only alter the constant K_1 in Eq. (14), and thus, as long as ξ is a constant. it will not matter what non-zero value is used for the prediction of E_v. Fig. 11 shows d/R as a function of ξ together with a linear dashed line to illustrate the linear dependence between d/R and ξ. The figure assumes $V_i = 5$ m/s, which is a high V_i in this work. The linearity further increases with decreasing velocity because the contribution of the contact pressure in Eq. (5) decreases.

As shown in Fig. 10, Eq. (14) provides a good fit to the experimental measurements for the ice particles with a diameter of 1.64 mm ($R = 0.82$ mm). To address how e_n will scale with a change in particle size we extracted the values of e_n published by Higa et al. [27] for ice particles with radii of 1.4 mm and 4.0 mm at $T = 261$ K. These results together with the e_n predicted by the new model are shown in Fig. 12. Again the model captures the trend that is observed in the experiments.

3.2. General regime map for the coefficient of restitution of ice particle collisions

The measurements we have presented complement existing measurements and lead us to propose a regime map for ice collisions. We identify three e_n regimes for ice particle collisions: an intermolecular adhesive regime, a collisional melting regime, and a fragmentation regime. The intermolecular adhesive regime is characterized by damping due to intermolecular forces. In previous work [31], we studied when an ice particle sticks or bounces depending on intermolecular forces. Based on the Johnson-Kendall-Roberts (JKR) model, at low V_i, e_n can be defined as,

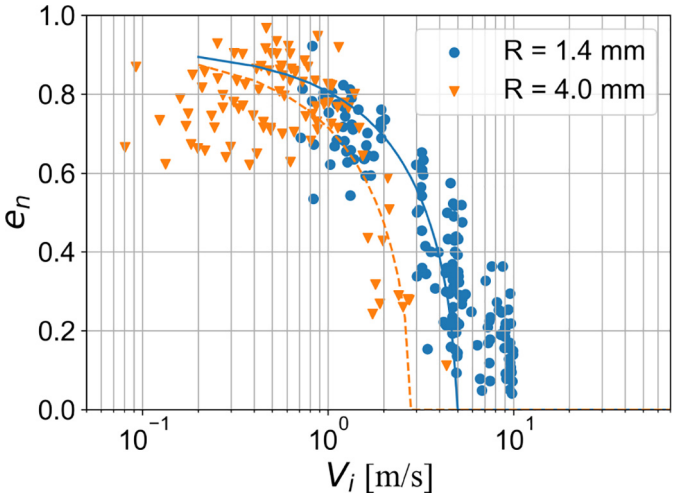

Fig. 12. The e_n for ice particles colliding with an ice wall at $T = 261$ K. Scattered with circles and triangles show experimental results published in Higa et al. [27] for radii 1.4 mm and 4.0 mm respectively. Dashed and solid lines show the novel model predictions for 1.4 mm and 4.0 mm radii, respectively.

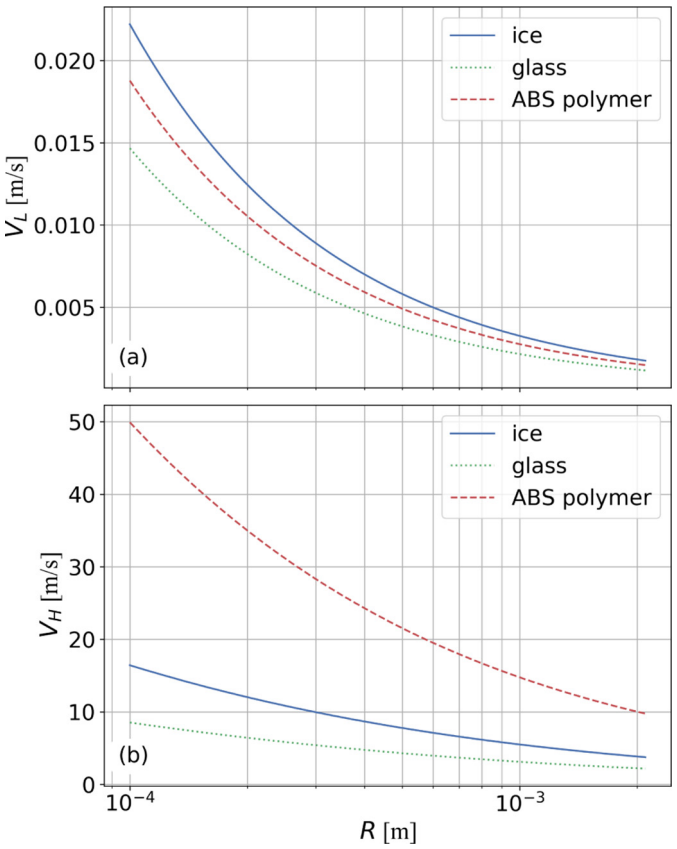

Fig. 13. The sticking velocities V_L (a) and V_H (b) for ice particles colliding with different massive walls as a function of R at $T = 261$ K. Solid, dashed and dotted lines shows the calculated sticking velocities for ice particles colliding with an ice wall, a polymer wall and a glass wall respectively. In (a) below each respective line particles sticking will occur. In (b) above each respective line particles sticking will occur.

$$e_n = \sqrt{1-\left(\frac{V_L}{V_i}\right)^2}, \tag{16}$$

where V_L is the lower sticking velocity and for collisional velocities below V_L, particles stick due to intermolecular adhesion. This lower sticking velocity is defined as,

$$V_L = \frac{3\sqrt{3}}{4}\sqrt{\frac{K_1}{\rho_s}}\left(\frac{\pi^2 W^5}{R^5 E^{*2}}\right)^{\frac{1}{6}}. \tag{17}$$

where $K_1 \approx 0.9355$ is an integration constant [31]. From Eq. (17) it can be seen that the V_L is mainly governed by the interaction properties E^* and W (work of adhesion), but will also increase with decreasing R. The collisional melting regime is defined by Eq. (15). In this regime an ice particle colliding with a massive wall will have a rapid increase in energy loss with increasing V_i until the particle begins to adhere to the wall. This will occur when the incoming kinetic energy is equal to the sum of energy causing damage at the interface and the energy lost due to viscous damping. This condition results in a separate, higher sticking velocity, V_H, that can be defined as,

$$V_H = \frac{3C}{2\pi(1-\xi)}\exp\left(\frac{G_0^+}{k_b T}\right)(d_H/\varepsilon)^{1.5}, \tag{18}$$

where d_H is the melted liquid layer thickness when this sticking occurs. However, d_H is a nonlinear function of V_i, as seen in Eq. (5) and therefore it is not possible to derive an explicit equation for the V_H and Eq. (18) can only be solved implicitly. In Fig. 13 the sticking velocities V_L and V_H are plotted as a function of R for ice particles colliding with an ice wall, a polymer wall and a glass wall at $T = 261$ K. As concluded by Eidevåg et al. [31], a polymer wall will have a higher V_L than a glass wall which means that a polymer wall will tend to accumulate more ice particles than a glass wall for V_i in the intermolecular adhesive regime. However, for high velocity collisions, where collisional melting dominates, a glass wall have a lower V_H than a polymer wall and therefore a glass wall is predicted to accumulate more ice particles than a polymer wall for V_i in the collisional melting regime.

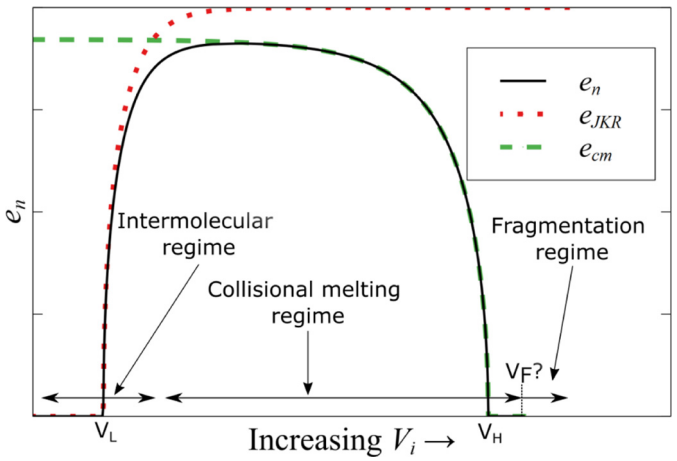

Fig. 14. The coefficient of restitution for ice particles upon collision with a massive wall. The red dotted line (e_{JKR}) shows the coefficient of restitution due to intermolecular forces. The dashed green line (e_{cm}) shows the coefficient of restitution due to collisional melting, and a fragmentation regime is also indicated where the e_n becomes undefined. The combined e_n is shown by the black solid line.

For even greater velocities ice particles will continue to adhere until fragmentation begins to influence the impacts at a certain fragmentation velocity V_F. Particles at these velocities, in excess of collisional fusion, will rebound but simultaneously fragment. Previous experiments have shown that for high velocity impacts, particles rebound and lose energy due to fragmentation but partial fragments may adhere to the wall [50]. Experimental data in this range is lacking and the e_n for such impacts is ill-defined given that the impacting particle will not remain intact.

The outlined regimes can be convoluted to yield a map for ice particle impacts (Fig. 14). In the figure, e_n is the convoluted coefficient of restitution that emerges from considering, e_{JKR} due to intermolecular forces and e_{cm} due to collisional melting. A fragmentation regime is indicated for velocities above an unknown V_F to illustrate that this is an experimentally unexplored region. The sticking velocities V_L and V_H are also indicated in the figure. The combined model predicts a horizontal plateau around the point $e_n = \sqrt{1-\xi^2}$ and this demostrates why previous studies have proposed a quasi-static regime for the e_n of ice particles. However, the new combined model also predicts that e_n will decrease for V_i below this point.

4. Conclusions

In this study we have investigated the damping mechanisms of ice particles that collide with walls, specifically in terms of the coefficient of restitution e_n. Experimental measurements of e_n for millimeter-sized particles at different temperatures and for different wall materials were presented. We obtain a velocity dependent e_n, similar to what has previously been observed by Higa et al. [27]. Different magnitudes of e_n for ice particles colliding with different wall materials were also obtained. Collisions with a polymer wall had the highest e_n and collisions with a hardened glass wall had the lowest e_n.

We propose that the rapid energy dissipation for ice particles colliding with walls can be explained by collisional melting and the associated viscous damping the increased premelted liquid-layer causes in a collision. A novel model has been derived that captures obtained temperature dependencies and observed differences attributed to wall material properties. We combined the new model with previous work [31] and proposed a regime map for the e_n of ice particles.

Nomenclature

e_n	normal coefficient of restitution (−)
V_i	normal impact velocity (m/s)
V_b	normal rebound velocity (m/s)
V_c	critical damping velocity (m/s)
V_L	lower sticking velocity (m/s)
V_H	higher sticking velocity (m/s)
d	liquid layer thickness (m)
ρ_s	density of solid water (kg/m3)
ρ_f	density of liquid water (kg/m3)
k_b	Boltzmann constant (eV/K)
E^*	effective Young's modulus (Pa)
T	experimental temperature (K)
T_m	melting temperature (K)
T_H	homologous temperature (−)
η	viscosity of the liquid layer (Pa-s)
ε	particle roughness length scale (m)
F_v	viscous force (N)
E_v	energy loss due to viscous damping (J)
R	particle radius (m)
W	work of adhesion (J/m2)
ξ	fraction of kinetic energy causing damage at interface (−)
q_m	latent heat of fusion (J)
δa	uncertainty of quantity a

Declaration of Competing Interest

The authors declare that they have no known competing financial interests or personal relationships that could have appeared to influence the work reported in this paper.

Acknowledgments

The authors are grateful to Arctic Falls AB for making their facilities available for the experiments. We thank Per Gren at Luleå University of Technology for his help with the experimental setup. This work was funded by VINNOVA (2017-03029). EST is supported by the Swedish Research Council FORMAS (2017-00564) and Swedish Research Council VR (2020-03497), and by the Swedish Strategic Research Area MERGE.

References

[1] J. Blum, Dust evolution in Protoplanetary discs and the formation of planetesimals, Space Sci. Rev. 214 (2018) 1–19, https://doi.org/10.1007/s11214-018-0486-5.
[2] J.G. Dash, B.L. Mason, J.S. Wettlaufer, Theory of charge and mass transfer in ice-ice collisions, J. Geophys. Res. 106 (2001) 395–415, https://doi.org/10.1029/2001JD900109.
[3] R.A. Schmidt, Properties of blowing snow, Rev. Geophys. 20 (1982) 39–44, https://doi.org/10.1029/RG020i001p00039.
[4] P.O.A. Borrebæk, B.P. Jelle, Z. Zhang, Avoiding snow and ice accretion on building integrated photovoltaics – challenges, strategies, and opportunities, Sol. Energy Mater. Sol. Cells 206 (2020)https://doi.org/10.1016/j.solmat.2019.110306.
[5] B.E.K. Nygaard, H. Ágústsson, K. Somfalvi-Tóth, Modeling wet snow accretion on power lines: improvements to previous methods using 50 years of observations, J. Appl. Meteorol. Climatol. 52 (2013) 2189–2203, https://doi.org/10.1175/JAMC-D-12-0332.1.
[6] P. Abrahamsson, M. Eng, A. Rasmuson, An infield study of road snow properties related to snow-car adhesion and snow smoke, Cold Reg. Sci. Technol. 145 (2018) 32–39, https://doi.org/10.1016/j.coldregions.2017.09.008.
[7] M. Sommerfeld, Modelling of particle-wall collisions in confined gas-particle flows, Int. J. Multiphase Flow 18 (1992) 905–926, https://doi.org/10.1016/0301-9322(92)90067-Q.
[8] S. Matsusaka, H. Maruyama, T. Matsuyama, M. Ghadiri, Triboelectric charging of powders: a review, Chem. Eng. Sci. 65 (2010) 5781–5807, https://doi.org/10.1016/j.ces.2010.07.005.
[9] C. Thornton, Granular Dynamics, Contact Mechanics and Particle System Simulations: A DEM Study, vol. 24, Springer International Publishing, 2015 https://doi.org/10.1007/978-3-319-18711-2.
[10] J. Marshall, S. Li, Adhesive Particle Flow: A Discrete-Element Approach, Cambridge University Press, Cambridge, 2014 https://doi.org/10.1017/CBO9781139424547.
[11] J. Marshall, Modeling and sensitivity analysis of particle impact with a wall with integrated damping mechanisms, Powder Technol. 339 (2018) 17–24, https://doi.org/10.1016/j.powtec.2018.07.097.
[12] R. Boettcher, S. Eichmann, P. Mueller, Influence of viscous damping and elastic waves on energy dissipation during impacts, Chem. Eng. Sci. 199 (2019) 571–587, https://doi.org/10.1016/j.ces.2019.01.036.
[13] S. Aman, P. Mueller, J. Tomas, S. Kozhar, M. Dosta, S. Heinrich, S. Antonyuk, Combined viscoelastic and elastic wave dissipation mechanism at low velocity impact, Adv. Powder Technol. 27 (2016) 1244–1250, https://doi.org/10.1016/j.apt.2016.04.012.
[14] K.L. Johnson, H.M. Pollock, The role of adhesion in the impact of elastic spheres, J. Adhes. Sci. Technol. 8 (1994) 1323–1332, https://doi.org/10.1163/156856194X00636.
[15] N.V. Brilliantov, T. Pöschel, Collision of adhesive viscoelastic particles, Phys. Granular Media (2005) 189–209, https://doi.org/10.1002/352760362X.ch8 arXiv:0506253v1.
[16] C. Thornton, Z. Ning, A theoretical model for the stick/bounce behaviour of adhesive, elastic- plastic spheres, Powder Technol. 99 (1998) 154–162, https://doi.org/10.1016/S0032-5910(98)00099-0.
[17] S. Antonyuk, S. Heinrich, N. Deen, H. Kuipers, Influence of liquid layers on energy absorption during particle impact, Particuology 7 (2009) 245–259, https://doi.org/10.1016/j.partic.2009.04.006.
[18] B. Buck, S. Heinrich, Collision dynamics of wet particles: comparison of literature models to new experiments, Adv. Powder Technol. 30 (2019) 3241–3252, https://doi.org/10.1016/j.apt.2019.09.033.
[19] F. Gollwitzer, I. Rehberg, C.A. Kruelle, K. Huang, Coefficient of restitution for wet particles, Phys. Rev. E – Statist. Nonlinear Soft Matter Phys. 86 (2012) 1–9, https://doi.org/10.1103/PhysRevE.86.011303 arXiv:1202.1750.
[20] V.S. Sutkar, N.G. Deen, J.T. Padding, J.A. Kuipers, V. Salikov, B. Crüger, S. Antonyuk, S. Heinrich, A novel approach to determine wet restitution coefficients through a unified correlation and energy analysis, AICHE J. 61 (2015) 769–779, https://doi.org/10.1002/aic.14693.
[21] M. Khalilitehrani, J. Olsson, A. Rasmuson, F. Daryosh, A regime map for the normal surface impact of wet and dry agglomerates, AICHE J. 64 (2018) 1975–1985, https://doi.org/10.1002/aic.16072.
[22] J.P. Dilley, Energy loss in collisions of icy spheres: loss mechanism and size-mass dependence, Icarus 105 (1993) 225–234, https://doi.org/10.1006/icar.1993.1120.
[23] K.D. Supulver, F.G. Bridges, D. Lin, The coefficient of restitution of ice particles in glancing collisions: experimental results for unfrosted surfaces, Icarus 113 (1995) 188–199, https://doi.org/10.1006/ICAR.1995.1015.
[24] I.V. Roisman, C. Tropea, Impact of a crushing ice particle onto a dry solid wall, Proceed. Roy. Soc. A: Math. Phys. Eng. Sci. 471 (2015) https://doi.org/10.1098/rspa.2015.0525.
[25] C.R. Hill, D. Heißelmann, J. Blum, H.J. Fraser, Collisions of small ice particles under microgravity conditions, Astron. Astrophys. 573 (2015) A49, https://doi.org/10.1051/0004-6361/201424069 arXiv:1411.0563.
[26] C. Güttler, D. Heißelmann, J. Blum, S. Krijt, Normal Collisions of Spheres: A Literature Survey on Available Experiments, URL: http://arxiv.org/abs/1204.0001 2012arXiv:1204.0001.
[27] M. Higa, M. Arakawa, N. Maeno, Size dependence of restitution coefficients of ice in relation to collision strength, Icarus 133 (1998) 310–320, https://doi.org/10.1006/icar.1998.5938.
[28] S.C. Colbeck, An overview of seasonal snow metamorphism, Rev. Geophys. Space Phys. 20 (1982) 45–61, https://doi.org/10.1029/RG020i001p00045.
[29] A. Langlois, A. Royer, B. Montpetit, A. Roy, M. Durocher, Presenting snow grain size and shape distributions in Northern Canada using a new photographic device allowing 2D and 3D representation of snow grains, Front. Earth Sci. 7 (2020) https://doi.org/10.3389/feart.2019.00347.
[30] J.S. Wettlaufer, Accretion in protoplanetary disks by collisional fusion, Astrophys. J. 719 (2010) 540–549, https://doi.org/10.1088/0004-637X/719/1/540.
[31] T. Eidevåg, P. Abrahamsson, M. Eng, A. Rasmuson, Modeling of dry snow adhesion during normal impact with surfaces, Powder Technol. 361 (2019) 1081–1092, https://doi.org/10.1016/j.powtec.2019.10.085.
[32] M. Vargas, P.M. Struk, R.E. Kreeger, J. Palacios, K.A. Iyer, R.E. Gold, Ice Particle Impacts on a Moving Wedge, 2013 https://doi.org/10.2514/6.2014-3045.
[33] B. Crüger, V. Salikov, S. Heinrich, S. Antonyuk, V.S. Sutkar, N.G. Deen, J.A. Kuipers, Coefficient of restitution for particles impacting on wet surfaces: an improved experimental approach, Particuology 25 (2016) 1–9, https://doi.org/10.1016/j.partic.2015.04.002.
[34] J.Y. Tinevez, N. Perry, J. Schindelin, G.M. Hoopes, G.D. Reynolds, E. Laplantine, S.Y. Bednarek, S.L. Shorte, K.W. Eliceiri, TrackMate: an open and extensible platform for single-particle tracking, Methods 115 (2017) 80–90, https://doi.org/10.1016/j.ymeth.2016.09.016.
[35] K.L. Johnson, Contact Mechanics, Cambridge University Press, Cambridge, 1985https://doi.org/10.1017/CBO9781139171731.
[36] B. Yildirim, H. Yang, A. Gouldstone, S. Müftü, Rebound mechanics of micrometre-scale, spherical particles in high-velocity impacts, Proceed. Roy. Soc. A: Math. Phys. Eng. Sci. 473 (2017) https://doi.org/10.1098/rspa.2016.0936.

[37] K. Hashemnia, Experimental study of the effect of temperature on the coefficient of restitution of steel balls impact to some industrial metal sheets at elevated temperatures, Powder Technol. 368 (2020) 170–177, https://doi.org/10.1016/j.powtec.2020.04.053.
[38] J. Grau-Bove, C. Mangwandi, G. Walker, D. Ring, K. Cronin, Studies into the effect of temperature on the impact of model particles in co-melt granulation, Powder Technol. 294 (2016) 411–420, https://doi.org/10.1016/j.powtec.2016.02.041.
[39] J.G. Dash, Haiying Fu, J.S. Wettlaufer, The premelting of ice and its environmental consequences, Rep. Prog. Phys. 58 (1995) 115–167, https://doi.org/10.1088/0034-4885/58/1/003.
[40] J.G. Dash, A.W. Rempel, J.S. Wettlaufer, The physics of premelted ice and its geophysical consequences, Rev. Mod. Phys. 78 (2006) 695–741, https://doi.org/10.1103/RevModPhys.78.695.
[41] T. Bartels-Rausch, H.W. Jacobi, T.F. Kahan, J.L. Thomas, E.S. Thomson, J.P. Abbatt, M. Ammann, J.R. Blackford, H. Bluhm, C. Boxe, F. Domine, M.M. Frey, I. Gladich, M.I. Guzmán, D. Heger, T. Huthwelker, P. Klán, W.F. Kuhs, M.H. Kuo, S. Maus, S.G. Moussa, V.F. McNeill, J.T. Newberg, J.B. Pettersson, M. Roeselová, J.R. Sodeau, A review of air-ice chemical and physical interactions (AICI): Liquids, quasi-liquids, and solids in snow, Atmos. Chem. Phys. 14 (2014) 1587–1633, https://doi.org/10.5194/acp-14-1587-2014.
[42] L. Benatov, J.S. Wettlaufer, Abrupt grain boundary melting in ice, Phys. Rev. E – Statist. Phys. Plasmas Fluids Related Interdiscip. Top. 70 (2004) 7, https://doi.org/10.1103/PhysRevE.70.061606 arXiv:0412747.
[43] E.S. Thomson, L. Benatov, J.S. Wettlaufer, Erratum: abrupt grain boundary melting in ice (Physical Review E - Statistical, Nonlinear, and Soft Matter Physics (2004) 70 (061606)), Phys. Rev. E – Statist. Nonliner Soft Matter Phys. 82 (2010), 61606, https://doi.org/10.1103/PhysRevE.82.039907.
[44] E.S. Thomson, H. Hansen-Goos, J.S. Wettlaufer, L.A. Wilen, Grain boundary melting in ice, J. Chem. Phys. 138 (2013) https://doi.org/10.1063/1.4797468 arXiv:1212.5508.
[45] S. Murakami, Continuum Damage Mechanics: A Continuum Mechanics Approach to the Analysis of Damage and Fracture, Springer, Netherlands, 2012https://doi.org/10.1007/978-94-007-2666-6.
[46] M.J. Matthewson, Adhesion of spheres by thin liquid films, Philosop. Magaz. A: Phys. Condens. Matter Struct. Defects Mech. Proper. 57 (1988) 207–216, https://doi.org/10.1080/01418618808204510.
[47] D.Y. Chan, R.G. Horn, The drainage of thin liquid films between solid surfaces, J. Chem. Phys. 83 (1985) 5311–5324, https://doi.org/10.1063/1.449693.
[48] R.B. Bird, W.E. Stewart, E.N. Lightfoot, Transport Phenomena, John Wiley & Sons Inc, 2006.
[49] P.V. Hobbs, Ice Physics, Oxford University Press, 1974.
[50] T. Hauk, I. Roisman, C. Tropea, Investigation of the impact behaviour of ice particles, 6th AIAA Atmospheric and Space Environments Conference, Atlanta, 2014 https://doi.org/10.2514/6.2014-3046.